# Investigation of turbulent thermal convection between horizontal plates

## By J. W. DEARDORFF AND G. E. WILLIS

National Center for Atmospheric Research, Boulder, Colorado

Properties of turbulent thermal convection were measured in air between horizontal plates maintained at constant temperatures. Rayleigh numbers of $6.3 \times 10^5$, $2.5 \times 10^6$ and $1.0 \times 10^7$ were studied with a convection chamber designed to allow measurements to be taken along a horizontal path. Vertical profiles are presented of horizontally averaged temperature; r.m.s. fluctuations of temperature, horizontal velocity and vertical velocity; total heat flux; the correlation coefficient between vertical velocity and temperature; all terms in the thermal variance equation; and of terms in the turbulent kinetic energy balance.

One-dimensional spectra of temperature, horizontal velocity and vertical velocity at two different heights all disclose large intensity for waves of length 5 to 15 times the plate separation. Secondary peaks occur for scales of from 0.7 to 1.7 times the separation height.

Many of the observations are consistent with a thermal structure dominated by plumes extending most or all of the distance between plates.

## Introduction

Thermal convection between large horizontal plates held at fixed temperatures can produce a basic kind of turbulence which has received very little detailed experimental study. The magnitude and dependence of the heat flux upon Rayleigh and Prandtl number is perhaps the best known property of the convection, largely as a result of studies by Silveston (1958) and Globe & Dropkin (1959). The mean temperature profile has been measured adequately by Thomas & Townsend (1957) for Rayleigh numbers of $0.85 \times 10^5$ and $3.8 \times 10^5$. Some temperature profiles have also been presented by Somerscales (1965), but the vertical asymmetry which was obtained seems highly unrealistic. A single profile of the temporal r.m.s. temperature fluctuations was presented by Thomas & Townsend, and several by Somerscales, but it is uncertain how much the short term variance at a fixed point underestimates the horizontally averaged, or long term, value. The only measurements of velocities are approximate, space-averaged observations by Malkus (1954a) which, however, covered the large Rayleigh number range from about $10^5$ to $10^9$.

Reliable measurements are needed of r.m.s. velocity component and temperature fluctuation as functions of height, analyses of power spectra and measurement of terms in the kinetic energy and thermal variance equations as a function

of height. Statistical averages should be taken with respect to a horizontal direction, rather than in time, in order to avoid the very long averaging times found by Deardorff & Willis (1965) to be necessary for their equivalence.

The present experimental study attempts to fulfil these requirements and to provide sufficient details against which theories and models of turbulent thermal convection may be tested. It is becoming evident that knowledge of the heat flux alone is insufficient to test adequately a theoretical model. For example, the heat flux in air at a Rayleigh number of $6.75 \times 10^5$ was predicted correctly within 5 % by a numerical model of Deardorff (1965), but comparison with results to be presented show that the r.m.s. vertical velocities and temperature fluctuations were predicted to be about 50 % too small and large, respectively. It is not the purpose of this paper, however, to compare results with theory, although some qualitative explanation will be advanced to relate certain observations to more fundamental ones.

The experimental results to be presented are for a Prandtl number of 0·71 (air) and for Rayleigh numbers of $6.3 \times 10^5$, $2.5 \times 10^6$ and $1.0 \times 10^7$. The restriction to air resulted from the desire to measure velocities accurately by hot-wire techniques. The lower limit of Rayleigh number was set by the minimum distance between horizontal plates in which a roving hot-wire probe could be conveniently mounted and positioned, and by the minimum plate temperature difference which could be accurately measured. The upper limit of Rayleigh number was set by the maximum plate separation compatible with a large plate width in comparison with plate separation, and by the maximum plate temperature difference compatible with the desire for nearly constant molecular properties. It would be valuable, of course, to pursue similar measurements for fluids of widely different Prandtl number, and to treat much higher Rayleigh numbers.

## 1. Convection chamber

The chamber was designed around the objective of moving the velocity and temperature sensors uniformly in a horizontal direction through air at heights ranging from just below mid chamber level to a level just below the upper plate. The chamber length is 366 cm, width 94 cm, and height adjustable from about 4 cm to 30 cm. The sensors could be moved along the longitudinal, or $x$, direction over a distance of about 300 cm. The length was designed greater than the width to allow the longest practicable continuous data sample from any single traverse of the probes.

Figure 1 is a drawing of the chamber in which most of the main features are denoted. The system for providing the plate temperature difference (not visible in the figure) consists mainly of two insulated 120-litre reservoirs which serve as mixing chambers for water circulated adjacent to the top and bottom plates of the chamber. Warm water is pumped through aluminium channels just beneath the lower plate, is collected and passed through a water heater, and returned to the warm reservoir. Cool water from the other reservoir is circulated within identical channels just above the upper plate of the chamber, is collected and then

cooled by passage over refrigerator coils, and returned to the cool reservoir. The channels for the circulating water extend the length of the chamber and are 3·1 cm in interior width and 1·3 cm in depth. The flow direction is opposite in
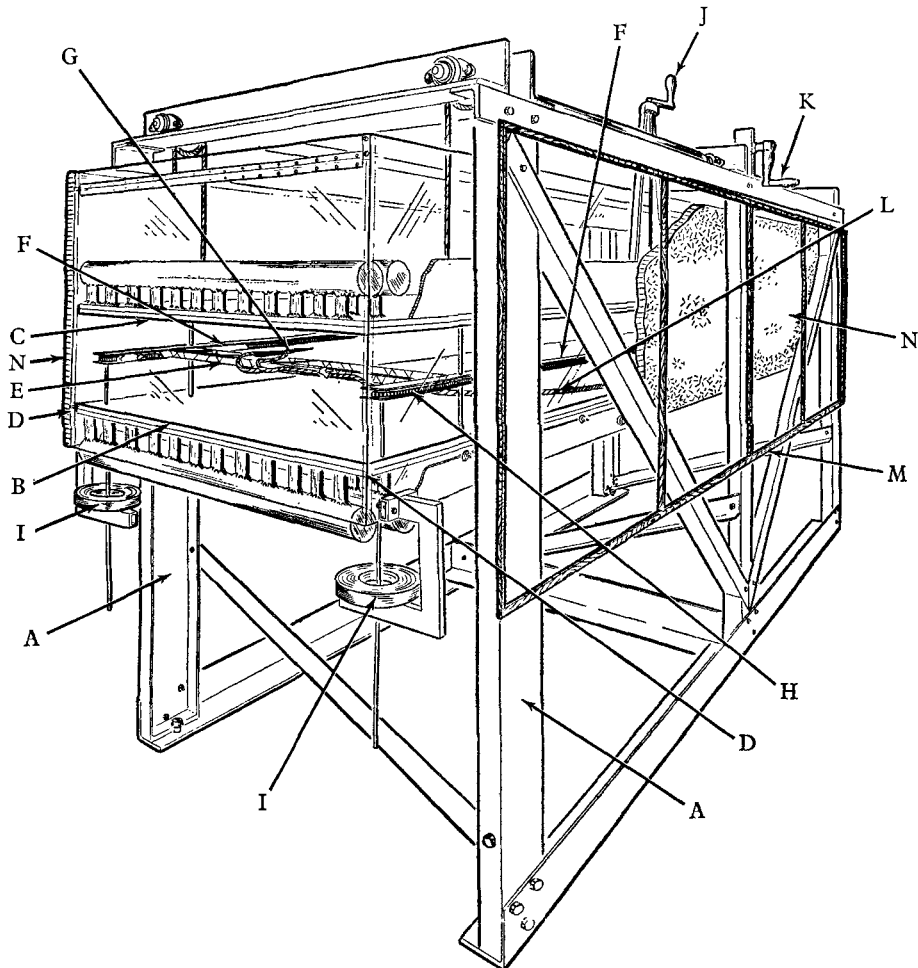


FIGURE 1. Drawing of the convection chamber as viewed from one corner. Letters designate the following features: A, supporting beams (aluminium) of chamber; B, lower horizontal plate (aluminium of 1·3 cm thickness); C, upper plate (face not visible); D, Plexiglass side walls of 1·3 cm thickness; E, probe-support frame; F, tracks which support the movable frame; G, hot-wire and/or resistance-wire probe in position to commence a traverse; H, chain drive for moving the probe-support frame longitudinally; I, flywheels to damp high-frequency oscillations; J, hand crank to position track and probe vertically; K, hand crank to change the plate separation; L, electrical cable from sensors of probe; M, wooden frame (in storage) which, when strung with a long resistance wire, measured the horizontally averaged temperature; N, fibre-glass insulation of 5 cm thickness which covered the two long Plexiglass side walls during measurements.

adjacent channels in order to provide constant temperatures in the longitudinal direction at the interior surfaces of the plates.

The plates are aluminium of 1·3 cm thickness. Plate temperatures measured inside the chamber in a transverse direction along the chamber width showed no

detectable (less than 0·01 °C) small-scale variations associated with the opposite flow directions in adjacent channels exterior to the plates; however, a gradual increase of plate temperature difference, reaching 4·4 %, was noted in progressing from the sidewalls to the chamber interior in spite of the outer insulation of the chamber. This insulation consisted of fibre-glass exterior of the two longest Plexiglass walls.

A plate temperature difference, $\Delta T$, ranging from 2 to 25 °C or more could be maintained constant within 2 % over experimental periods of 5 to 10 hours. The temperature differences were measured with copper-constantan thermo-couples located in the circulating water supplied to the channels adjacent to the plates. Comparison against plate temperature differences measured by thermo-couples in direct contact indicated that the former were larger by amounts close to 5 %. This correction in $\Delta T$ was applied in obtaining the Rayleigh number

$$Ra = gh^3 \Delta T / T_m \nu_m \kappa_m,$$

where $g$ is the acceleration of gravity, $T_m$ the average chamber temperature, $h$ the plate separation, $\nu_m$ the mean kinematic viscosity and $\kappa_m$ the mean thermal diffusivity of air.

Temperature measurements of water circulating from the reservoirs to the convection chamber disclosed no detectable fluctuations, but only gradual drifts of typical magnitude 0·1 °C/hour. The chamber could be 'inverted' (for calibration purposes of utilizing a stable temperature gradient within the chamber) by interchanging the circulating water supplies. The external rates of heating and cooling of the circulating water of the chamber were set during experiments so that the mean chamber temperature, $T_m$, was nearly constant and equal to the average room temperature.

Other components of the chamber not shown in figure 1 are the drive motor and coupling for the moving probe system, limit switches for stopping the probe upon completion of a traverse and upon completion of its return, and the take-up mechanism for the electrical cable when the probe moves.

The chief difficulty encountered with the entire system was the occurrence of mechanical vibrations of the moving probe. The vibrations were associated with a chain-link drive system, and caused appreciable error signals in preliminary hot-wire anemometer measurements. They were later suppressed by proper adjustment of various chamber components, and by installation of four fly-wheels, two of which are visible in figure 1. Remaining vertical vibrations were larger than longitudinal ones, probably because of amplification associated with extension of the probe forward of its support frame, as in figure 2. However, the ratio of the r.m.s. error signal to the r.m.s. vertical velocity in the most unfavourable case was only 4 %; for most of the traverses it was about 0·5 %.

## 2. Measurement sensors

### 2.1. *Hot-wire anemometer*

The passage of the probe longitudinally through the air served, in addition to providing reliable averages, to provide a basic flow speed upon which the convective motions were superimposed as seen by the hot-wire anemometer. This

speed was set at 25·2 cm/sec, which is just over four times larger than the largest r.m.s. velocity component measured.

The hot-wire probe† had a greater diameter of about 7 mm with a tapered nose as shown in figure 2, plate 1. To measure the longitudinal velocity component, $u^*$, and vertical component $w^*$, the probe was equipped with $X$-wires oriented at about $\pm 45°$ from the horizontal and separated laterally by 1·5 mm. The wires were an alloy of 80 % platinum and 20 % iridium, with lengths of 2·0 mm and diameter $5·1 \times 10^{-3}$ mm. They were operated at a constant temperature of about 470 °C by means of two hot-wire amplifiers.‡ The sum and difference signals of the $X$-wire array, here denoted by $S$ and $D$, respectively, were recorded on the strip chart of a two-channel amplifier-recorder.§ The velocity components $u^*$ and $w^*$ were related primarily to $S$ and $D$ through empirical calibration constants.

In the calibration for $u^*$, the probe in horizontal orientation was passed through the chamber at various speeds centred at 25 cm/sec at times when no convective motions were present, and the sum signals recorded. There resulted a linear dependence of voltage signal upon longitudinal air speed, for probe speeds covering the rather wide range from 10 to at least 42 cm/sec. This linearity was unexpected, in that studies of Collis & Williams (1959) show a rather abrupt transition from the mixed flow region of combined free wire convection and forced convection to the forced convection region, where King's (1914) law approximately holds. The linearity may have been associated with a much smaller wire length-to-diameter ratio than that used by Collis & Williams. The calibration was not checked for air speeds greater than 42 cm/sec because of limitations of the probe drive mechanism, but the effect of free convection from the wire at speeds less than 10 cm/sec caused a gradual departure from linearity. A linear extrapolation below 10 cm/sec would indicate, for example, an air speed of 7·2 cm/sec at a true air speed of 6 cm/sec. However, these smaller speeds ($u^* < -15$ cm/sec) were rarely encountered by the moving probe even at the largest Rayleigh number where the maximum standard deviation of $u^*$ was 5·4 cm/sec.

Although the $X$-wires were heated to a relatively high temperature, a dependence of the sum signal upon ambient air temperature fluctuations was detectable. Two independent methods were used to obtain this temperature dependence. First, the probe was placed in a low speed jet of about 25 cm/sec from a combination fan and heater, and the air temperature was increased from 1 to 4 °C as measured by a thermocouple while the speed was held constant. In the second method the convection chamber was stably stratified and the probe passed through at constant speeds but at different levels where different mean temperatures prevailed. The average temperature dependence from the two methods agreed within 10 %, and the mean value from both methods was used in the calibration equation for $u^*$.

Another factor which affected the sum signal was the influence of the heated wake from one wire upon the other wire in the presence of a lateral velocity com-

† Disa Elektronic, Herlev, Denmark.
‡ Obtained from L. T. Miller, 310 Register Ave., Baltimore, Maryland.
§ Type RS Dynograph manufactured by Offner Division of Beckman Instruments, Inc., 3900 River Road, Schiller Park, Illinois.

ponent $v^*$. This effect is independent of the sign of $v^*$, and the correction term found to apply is proportional to $v^{*2}$.

The final calibration equation used for the sum signal is

$$\tfrac{1}{2}S \text{ (millivolts)} = -4{\cdot}34u^* \text{ (cm/sec)} + 2{\cdot}0T^{*\prime} \text{(degC)}$$
$$-0{\cdot}079[v^{*2} - \langle v^{*2}\rangle](\text{cm}^2/\text{sec}^2), \qquad (1)$$

where the prime denotes a fluctuation from the longitudinal mean, which in turn is denoted by angular brackets $\langle \; \rangle$. The velocity components were assumed to have negligible mean values. The correction terms involving $T^{*\prime}$ and $v^{*2}$ typically contributed 4 and 0·5 %, respectively, to the variance of $\tfrac{1}{2}S$.

In the calibration for $w^*$, the probe and its support frame were rotated at various angles up to $\pm 30°$ from the horizontal during traverses at constant speeds near 25 cm/sec, and during conditions of no thermal convection in the chamber. The influence of air temperature fluctuations upon the wire difference signal was found to be undetectable, as should be expected. The effect of a lateral velocity component in causing a heated wake from one wire to affect the other was quite appreciable, however. The calibration equation obtained for the difference signal, $D$, is

$$D \text{ (millivolts)} = 2{\cdot}94w^* \text{ (cm/sec)} + 1{\cdot}32v^* \text{ (cm/sec)}. \qquad (2)$$

(1) and (2) applied to the case when the probe was oriented longitudinally. However, the hot wires could not be passed very close to the upper plate of the chamber unless the probe was inclined slightly from the horizontal. For traverses within 2·8 cm of the upper plate, the probe was inclined at a 6° angle. This inclination understandably produced no detectable change in the leading terms in (1) and (2) involving $u^*$ and $w^*$, but did cause some of the $u^*$ component to appear in the difference signal. For measurements close to the upper plate, the equation which replaced (2) is

$$D \text{ (millivolts)} = 2{\cdot}94w^* \text{ (cm/sec)} + 0{\cdot}58u^* \text{ (cm/sec)} + 1{\cdot}32v^* \text{ (cm/sec)}, \qquad (3)$$

with (1) remaining essentially unchanged. Here the terms involving $u^*$ and $v^*$ typically contributed 2 and 9 %, respectively, to the variance of $D$. Vertical profiles of r.m.s. $u$ and $w$ values to be presented later show no discontinuities in the region where (3) replaced (2).

The calibration constant in front of $w^*$ in (2) or (3) did not depend upon probe angle. Hence for speeds of about 25 cm/sec, variations in wire heat loss due to varying wire orientation with respect to the direction of gravity during calibration were insignificant in comparison with variations associated with mean flow variations.

The calibration constants in these equations are averages from two separate calibrations taken within a day before and after the measurements with $Ra = 2{\cdot}5 \times 10^6$ and $1{\cdot}0 \times 10^7$. Slightly different constants apply to the measurements with $Ra = 6{\cdot}3 \times 10^5$. Values of the leading constants in these equations typically changed $\pm 4$ % from one calibration to the next.

## 2.2. *Resistance thermometer*

In order to measure fluctuating temperatures at nearly the same point in space as the velocity components, a narrow probe of 3 mm greatest diameter, with a resistance wire located between two needles of length 5 mm at its end, was soldered to the side of the $X$-wire probe previously described. The wire length was oriented horizontally and transversely, and centred 2·3 mm below the centroid of the $X$-wires. This wire† was a platinum alloy with 10 % rhodium, and with etched length 1·2 mm and diameter $1·3 \times 10^{-3}$ mm. Its resistance was about 225 ohms, and it was placed in a d.c. bridge network and supplied with 0·25 milliamperes. This current was found to be sufficiently small that the resistance-wire signal responded only to ambient temperature fluctuations and not detectably to velocity fluctuations.

For calibration, the resistance-wire probe and an adjacent copper-constantan thermocouple were subjected to gradual air temperature changes in a constant velocity flow of about 25 cm/sec. The response time of the resistance wire was well below a millisecond, but the effective time constant of the strip-chart recorder used in the experiments was about 0·01 sec.

## 2.3. *Temperature-gradient sensor*

The probe shown in figure 2 was utilized to obtain fluctuating temperature differences during longitudinal traverses. At the probe tip, two parallel etched resistance wires were mounted in a plane perpendicular to the longitudinal direction of the chamber. The wires were similar to the single resistance wire previously described, but had to be very carefully matched electrically in order that their difference signal corresponded only to a temperature difference over their separation interval. A wire separation of 2·1 mm appeared to be sufficiently small to enable the true mean-square vertical gradient, $\langle(\partial T^{*\prime}/\partial z^*)^2\rangle$, to be measured directly. This probe was calibrated by individual calibrations of the two wires in the same manner as the single resistance wire. A check of the calibration was obtained by comparing $\langle(\partial T^*/\partial y^*)^2\rangle$ from this probe with $\langle(\partial T^*/\partial x^*)^2\rangle$ obtained by longitudinal differentiation of the signal from the single wire during a traverse. The two quantities should be equivalent because of the horizontal isotropy of the thermal convection, and average agreement within 12 % was obtained. Because of this near agreement, the horizontal isotropy assumption was considered valid, and this probe was not utilized to obtain $\langle(\partial T^*/\partial y^*)^2\rangle$.

## 2.4. *Measurement of horizontally averaged temperature*

The temperatures measured by the resistance-wire sensor described in §2.2 could have been averaged longitudinally to obtain mean temperature as a function of height. However, it was found that an average from 4 or 5 traverses at each level would have been required to reduce sampling error to a tolerable level. Therefore a long nickel resistance wire was stretched back and forth diagonally six times at a given level within the chamber to produce a signal proportional to the

† Obtained from Sigmund Cohn Corporation, Mount Vernon, New York.

horizontally averaged temperature. The wire, of diameter 0·076 mm, was strung on the thin wooden frame shown in figure 1 (item M), and was held taut by constant tension. This frame was placed atop the track F of figure 1, so that the height of measurement could be varied easily from a level just grazing the upper plate to a level somewhat below mid chamber.

The long resistance wire was calibrated in the following manner. With convective turbulence present, the mean temperature very near a smooth horizontal boundary is known to be linear with height, and to be practically constant in the central portion of the chamber. With only a slight extrapolation with height, the signal from the long wire corresponding to the upper plate temperature was obtained. The second reference temperature to complete the calibration was obtained by assuming the nearly constant signal at mid level to correspond to the mean temperature between the two plates. The calibration by this method agreed within 4 % of that obtained by comparing the long-wire signals with thermocouple temperatures at the same height within the chamber during inversion conditions.

## 3. Data collection and analysis

Two longitudinal traverses were taken with the combination hot-wire anemometer and resistance thermometer at each of from 26 to 39 levels below the upper plate at each Rayleigh number. Data from the lower 40 % of the chamber were not collected because it was believed safe to assume symmetry of the statistics of the turbulence about mid chamber level. This assumption is supported by the fact that the mean air temperature at mid chamber level corresponded to the average of the two plate temperatures as mentioned in §2.4, and by the approximate constancy with height of the measured total heat flux to be discussed in §4. Two 2-channel strip-chart recorders were used simultaneously to obtain the hot-wire sum signal on one strip chart and the temperature and hot-wire difference signals on the other. From these records the r.m.s. values and spectra were obtained. Successive traverses were taken at about 3 minute intervals. Tests conducted with traverses taken more frequently disclosed no apparent effect of a given traverse upon the subsequent one if the interval between them was one half minute or more.

Typical results of traverses with the hot-wire anemometer at levels of $z^*/h = 0.91$ and $0.51$ are shown in figure 3 for a Rayleigh number of $2.5 \times 10^6$. $T'$ is a dimensionless temperature fluctuation, $\tilde{w}$ is proportional to the hot-wire difference signal and is roughly equal to the vertical velocity in dimensionless units, and similarly $\tilde{u}$ is roughly equal to the dimensionless longitudinal velocity component. Quantities have been made dimensionless by $\Delta T$, $h$ and $\kappa_m$. The asterisks, which refer to dimensional variables, will be omitted for the dimensionless variables. The abscissa of figure 3 is here considered proportional to longitudinal distance only, and not also proportional to time, because the probe speed was several times the r.m.s. velocities.

The temperature trace for $z^*/h = 0.91$ shows a negative skewness associated with cool air leaving the proximity of the upper plate in narrow regions. The

skewness is not present, of course, at $z^*/h = 0.51$. At this level the positive correlation between $T'$ and $\tilde{w}$ is evident, as is also the lack of significant correlation between $\tilde{w}$ and $\tilde{u}$.

Data from the strip charts were converted to digital form onto punched cards by means of a digital data analyzer.† The interval between successive data points correspond to 1·0 cm in the longitudinal direction, and to 0·04 sec in time. Each
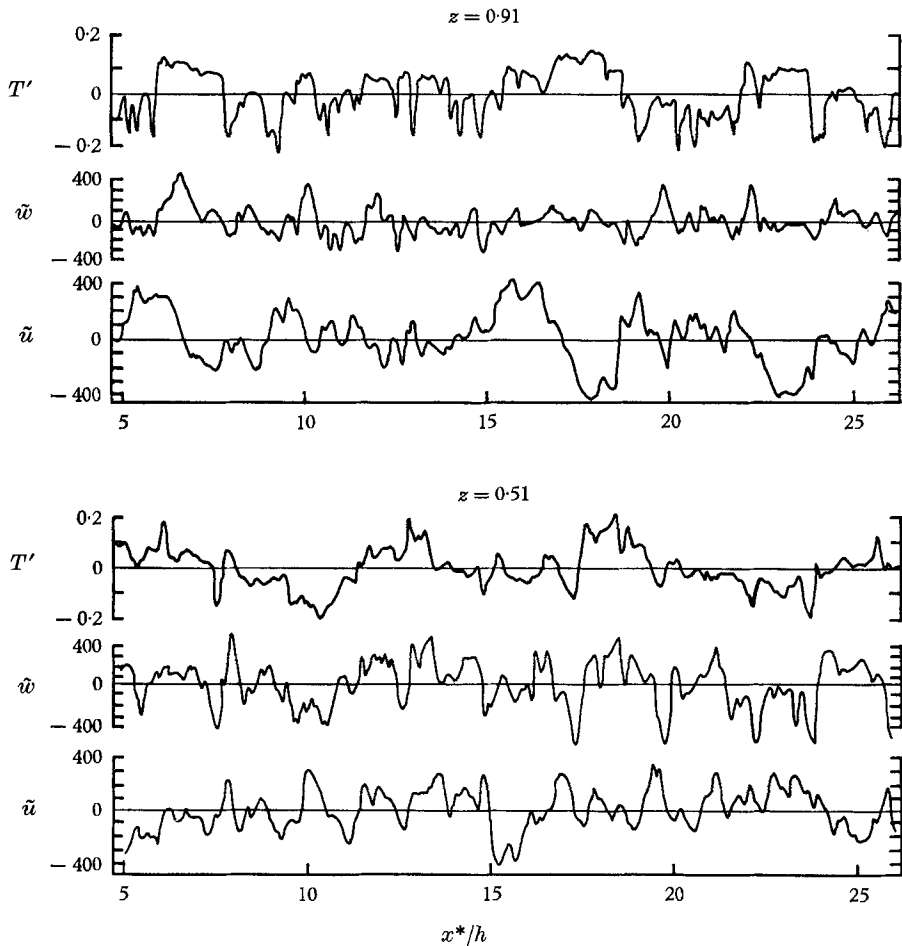


FIGURE 3. Typical records of fluctuations in $T$, $\tilde{w}$ and $\tilde{u}$ at two levels for $Ra = 2.5 \times 10^6$.

traverse resulted in 252 data points for each quantity measured; approximately the first 40 cm of each traverse was not analyzed because the drive motor required about 2 sec to accelerate the probe to the constant speed of 25·2 cm/sec.

Relevant physical parameters associated with the data collection at the three different Rayleigh numbers are given in table 1. $P_m$ is the air pressure, and the transverse aspect ratio is the ratio of chamber width to plate separation, $h$. Longitudinal aspect ratios were 3·9 times larger.

† Gerber Scientific Instrument Co., Hartford, Connecticut.

To obtain statistics of the thermal convection involving $u$ or $w$, both (1) and (2), or (1) and (3) had to be utilized simultaneously, along with knowledge of the temperature fluctuations and of certain statistics associated mainly with horizontal isotropy. For example, to obtain $\langle w^2 \rangle$ and $\langle u^2 \rangle$, we square (2) and average longitudinally to obtain

$$\langle D^2 \rangle = (2{\cdot}94)^2 \langle w^{*2} \rangle + (1{\cdot}32)^2 \langle u^{*2} \rangle,$$

upon assuming from horizontal isotropy that

$$\langle v^2 \rangle = \langle u^2 \rangle \quad \text{and} \quad \langle vw \rangle = 0. \qquad\qquad (4a,\,b)$$

| $Ra$ | $\Delta T$ (C) | $h$ (cm) | $T_m$ (K) | $\nu_m$ (cm²/sec) | $\kappa_m$ (cm²/sec) | $P_m$ (milli-bars) | Transverse aspect ratio |
|---|---|---|---|---|---|---|---|
| $6{\cdot}3 \times 10^5$ | 9·5 | 10·0 | 298 | 0·187 | 0·263 | 842 | 9·4 |
| $2{\cdot}5 \times 10^6$ | 21·6 | 12·0 | 299 | 0·188 | 0·264 | 841 | 7·8 |
| $1{\cdot}0 \times 10^7$ | 25·8 | 18·0 | 297 | 0·186 | 0·261 | 843 | 5·2 |

TABLE 1

The average square of (1) is

$$\langle (\tfrac{1}{2}S)^2 \rangle = (4{\cdot}34)^2 \langle u^{*2} \rangle + (2{\cdot}0)^2 \langle T^{*\prime 2} \rangle + (0{\cdot}079)^2 \times 2\langle u^{*2} \rangle^2,$$

upon making the Gaussian assumption that

$$\langle u^4 \rangle = 3\langle u^2 \rangle^2 \qquad\qquad\qquad (5)$$

and also assuming 
$$\langle uT \rangle = 0, \qquad\qquad\qquad (6)$$

$$\langle uv^2 \rangle = 0, \qquad\qquad\qquad (7)$$

$$\langle v^2 T' \rangle = 0. \qquad\qquad\qquad (8)$$

Assumption (6) follows from horizontal isotropy, but (7) and (8) were not checked. Assumption (5) enters only into the last term in the expression for $\langle (\tfrac{1}{2}S)^2 \rangle$ which contributes typically only 0·5 % to the variance of $\tfrac{1}{2}S$. The validity of (5) will be examined in the next section.

From the above equations for the averaged square sum and difference signals, both $\langle w^2 \rangle$ and $\langle u^2 \rangle$ are easily obtained after evaluation of $\langle T'^2 \rangle$. The averaging and evaluation of the statistics were performed numerically with a digital computer. Results to be presented in §4 represent averages from the two traverses made at each level.

In addition to the assumptions already listed, many others had to be made to evaluate other statistical properties from the impure hot-wire signals. These are:

$$\langle uw \rangle = 0, \quad \langle uv \rangle = 0, \quad \langle vT \rangle = 0, \qquad\qquad (9a,b,c)$$

$$\langle uT'^2 \rangle = 0, \quad \langle vT'^2 \rangle = 0, \qquad\qquad (9d,e)$$

$$\left\langle v \frac{\partial v}{\partial x} \frac{\partial u}{\partial x} \right\rangle = 0, \quad \left\langle v \frac{\partial v}{\partial x} \frac{\partial T}{\partial x} \right\rangle = 0, \quad \left\langle \frac{\partial u}{\partial x} \frac{\partial T}{\partial x} \right\rangle = 0, \qquad (9f,g,h)$$

$$\langle(\partial v/\partial y)^2\rangle = \langle(\partial u/\partial x)^2\rangle, \tag{9\,i}$$

$$\langle(\partial w/\partial y)^2\rangle = \langle(\partial w/\partial x)^2\rangle, \tag{9\,j}$$

$$\langle(\partial w/\partial z)^2\rangle = \langle(\partial u/\partial x)^2\rangle, \tag{9\,k}$$

$$\langle(\partial v/\partial x)^2\rangle = \langle(\partial u/\partial y)^2\rangle = 2\langle(\partial u/\partial x)^2\rangle, \tag{9\,l}$$

$$\langle(\partial u/\partial z)^2\rangle = \langle(\partial v/\partial z)^2\rangle = 2\,\langle(\partial u/\partial x)^2\rangle\,[\langle(\partial T'/\partial z)^2\rangle/\langle(\partial T/\partial x)^2\rangle]. \tag{9\,m}$$

Assumptions $(9\,a{-}c)$ again follow from horizontal isotropy. Those of (7), (8) and $(9\,d,e)$ may not be strictly true, but are sufficiently accurate if only small correlations exist between $T'^2$ and $u$ or $v$. Assumptions $(9\,f{-}m)$ are associated with estimation of the rate of dissipation of kinetic energy; only $(\partial u/\partial y)^2$ and $(\partial w/\partial x)^2$ were measured approximately out of the nine derivatives entering into the quantity. Attempts to measure $(\partial u/\partial y)^2$ and $(\partial u/\partial z)^2$ directly with a difference probe were abandoned upon noting the strong dependence of the signal upon a small angular difference between the two wires. Assumptions $(9\,h{-}j)$ again make use of horizontal isotropy, while $(9\,k{-}l)$ are strictly true only for fully three-dimensional isotropy. Assumption $(9\,m)$ utilizes a close similarity between the vertical distributions of $u$ and $T$ fluctuations to be noted in §4.

Besides evaluation of longitudinally averaged properties of the turbulence, part of the analysis consisted of one-dimensional Fourier analyses along the longitudinal direction. Fourier coefficients were obtained numerically for waves of length ranging from the length of record (254 cm) down to twice the data interval of 1 cm. The analysis is appropriate only if the data is cyclic, which, of course, rarely occurred. Therefore, for the purpose of this analysis only, the initial and final 5 % of the data traces were adjusted so as to give cyclic conditions by the following formula:

$$\tilde{T}(n) = T(n) - \{T(1) - \tfrac{1}{2}[T(1) + T(N)]\}\left[1 - \sin\frac{\pi(n-1)}{2\times 0.05N}\right], \tag{10}$$

where $\tilde{T}(n)$ is the revised value, $n$ is a data point index integer, and $N$ is the total number of data points from a traverse. An analogous formula applies for the final 5 % of record. Thus both end points were adjusted smoothly to the mean of their original values. Comparisons of spectra computed with and without the use of (10) showed no appreciable differences except that when a significant end-point discontinuity was originally present, spurious harmonics appeared at the higher wave numbers.

The squared sums of the Fourier sine and cosine coefficients were averaged over successive wave harmonics, $i$, for $i \geqslant 17$, in order to increase their statistical significance. The number averaged together ranged from 6 centred at $i = 19.5$ to 30 at $i = 107$. In addition, individual spectra from 8 traverses at similar heights were subsequently averaged together to produce the final spectra presented in §5.

## 4. Longitudinally averaged statistics

It should be emphasized that in the statistics to be presented, heights are made dimensionless by the plate separation $h$, temperatures by the positive plate temperature difference, $\Delta T$, and velocities by $\kappa_m/h$. Original, dimensionless

variables, denoted by asterisks when necessary, may be recovered from the dimensionless ones through use of table 1.

Vertical profiles of horizontally averaged temperature, obtained from use of the long resistance wire, are shown in figure 4 for the three Rayleigh numbers. The profiles are each averaged from two, for which the resistance wire was
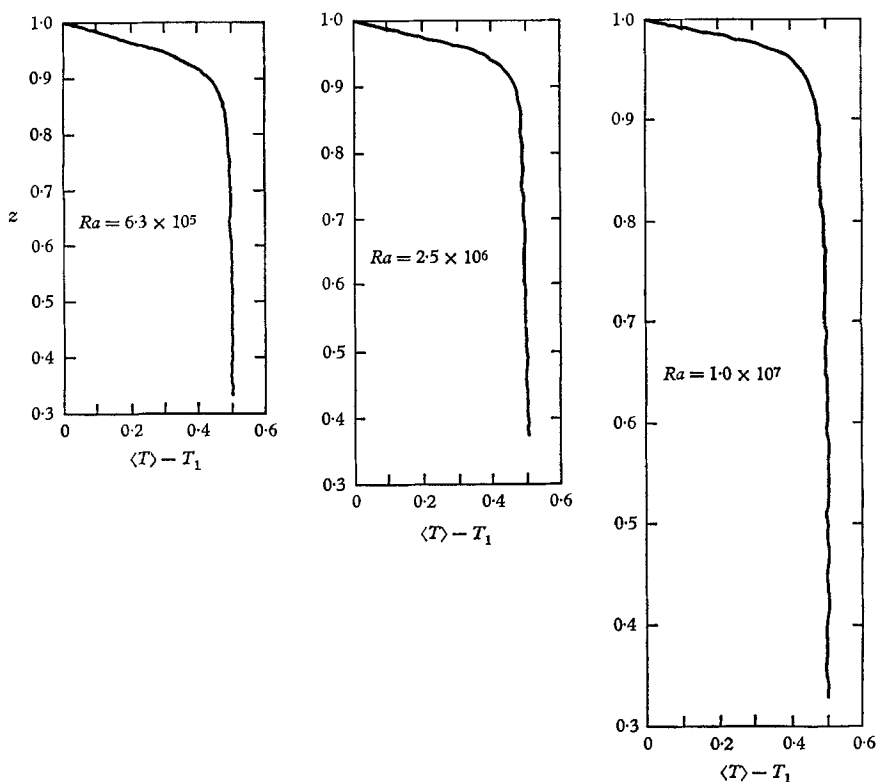


FIGURE 4. Vertical profiles of horizontally averaged temperature at three Rayleigh numbers.

gradually and continuously lowered from the upper plate to $z^*/h \equiv z \approx 0.4$, and then similarly returned. The small ripples reflect sampling errors even though the wire zigzagged within an $(x, y)$-plane of the chamber. The characteristic boundary layers and nearly isothermal central regions are evident. There is no suggestion of an inversion region at the edge of the boundary layer as might be inferred from measurements of Somerscales (1965) in silicone liquids. Such a region was also obtained by Thomas & Townsend (1957) in air at their largest Rayleigh number of $6.75 \times 10^5$, but was explained as being spuriously associated with their point sampling method and the presence of a quasi-steady large-scale circulation. Our profiles, and spectra to be presented in the next section, support their conclusion.

The region of steep boundary lapse rate merges rather abruptly into the nearly isothermal region in the vicinity of $0.8 < z < 0.95$ for these Rayleigh numbers. An examination of this region for possible power-law dependencies is reported elsewhere (Deardorff & Willis 1967). We have no explanation for the slight

temperature lapse in the central region at $Ra = 2.5 \times 10^6$ in view of its absence at the other two Rayleigh numbers.

Values of the Nusselt number, or dimensionless heat transport in the vertical direction: $Nu \equiv -\langle \partial T/\partial z\rangle + \langle wT\rangle$, are presented by data points in figure 5. Assumptions (6) and (9c) were used to equate $\langle \tilde{w}T\rangle$ to $\langle wT\rangle$. The quantity $Nu$ should be constant with height for the horizontally homogeneous and steady state, and appears to be so within the scatter of the data. The large spread of the data points indicates that the instantaneous heat flux averaged along a horizontal
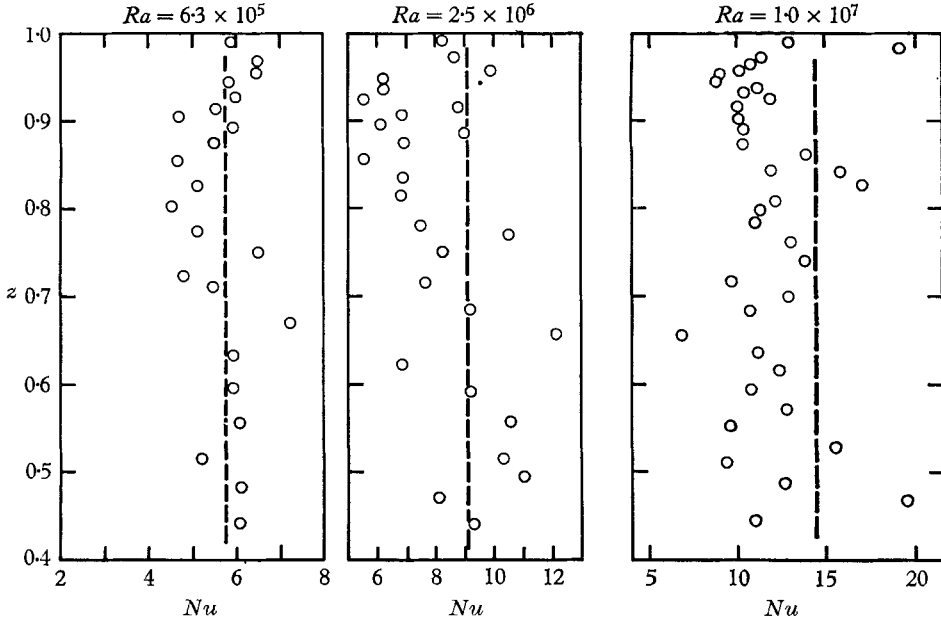


FIGURE 5. Measurements of total dimensionless heat flux $Nu \equiv \langle -\partial T/\partial z\rangle + \langle wT\rangle$ as a function of height. Vertical dashed lines are empirical values from Globe & Dropkin (1959).

line extending most of the chamber length may differ appreciably from the average over an entire horizontal plane. The vertical dashed lines are values given by the empirical formula of Globe & Dropkin (1959)

$$Nu = 0.069\,(Ra)^{\frac{1}{3}}\,(Pr)^{0.074}, \tag{11}$$

where $Pr$ is the Prandtl number. Values below $z \approx 0.8$ are associated almost entirely with the convective heat transport $\langle wT\rangle$, whereas the uppermost data point at each Rayleigh number is associated only with $-\langle \partial T/\partial z\rangle$ as close to the boundary as it could be estimated. The deviation of the vertically averaged values in figure 5 with respect to the values of Globe & Dropkin averages 8%. This approximate agreement suggests that the individual calibrations of the vertical velocity and temperature probes were accurate within perhaps $\pm 10\%$. The systematic underestimation of turbulent heat flux at the two higher Rayleigh numbers may result from the separation between $w$ and $T$ sensors.

Vertical profiles of $\sigma(T)$, $\sigma(u)$ and $\sigma(w)$, where $\sigma$ denotes the r.m.s. value, are shown in figures 6, 7 and 8 for the three Rayleigh numbers. The solid curves,

drawn by eye, indicate a remarkably close similarity between profiles of $\sigma(T)$ and
$\sigma(u)$ in air. Their maxima near the boundary suggests that large temperature
contrasts in this region are associated with horizontal 'mushrooming' of warm
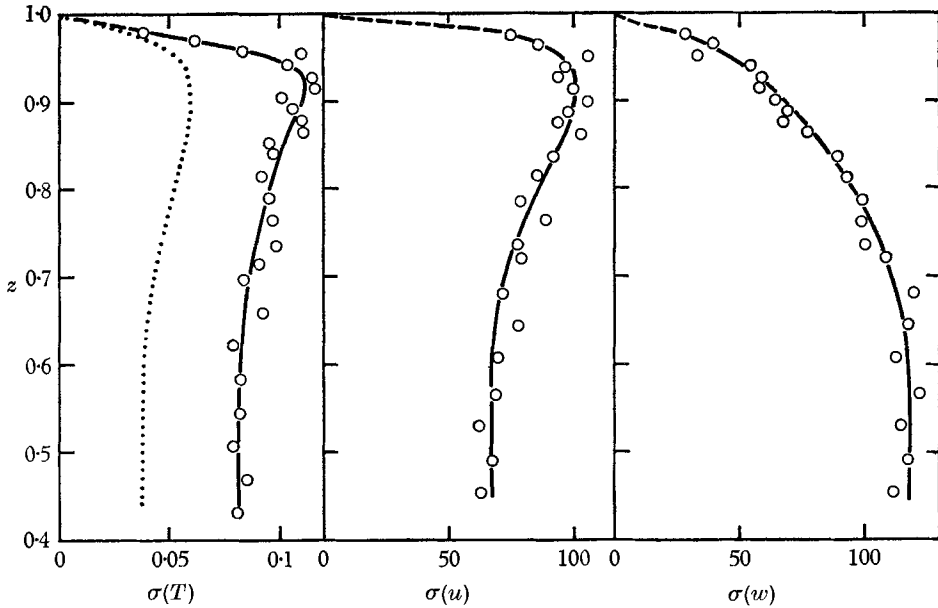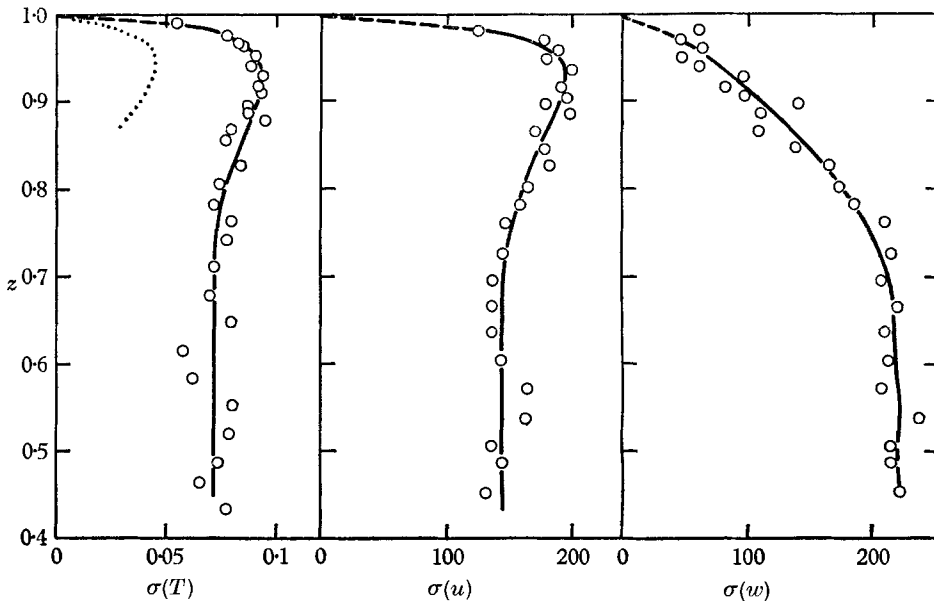air convected upwards from interior regions. Profiles of $\sigma(w)$ show a gradual



FIGURE 6. Vertical profiles of $\sigma(T)$, $\sigma(u)$ and $\sigma(w)$ at $Ra = 6.3 \times 10^5$. Dotted curve is $\sigma(T)$ from fixed-point measurements of Thomas & Townsend (1957) at $Ra = 6.75 \times 10^5$.



FIGURE 7. Vertical profiles of $\sigma(T)$, $\sigma(u)$ and $\sigma(w)$ at $Ra = 2.5 \times 10^6$. Dotted segment is $\sigma(T)$ from fixed-point measurements of Somerscales (1965) at $Ra = 2.0 \times 10^6$.

increase from zero at the boundary to a broad maximum at mid chamber level. These profiles are consistent with a structure in which the dominant eddies extend from plate to plate. The dimensionless depth of the boundary layer, whether defined from profiles of $\langle T \rangle$, $\sigma(T)$ or $\sigma(u)$, is seen to decrease with increasing Rayleigh number.
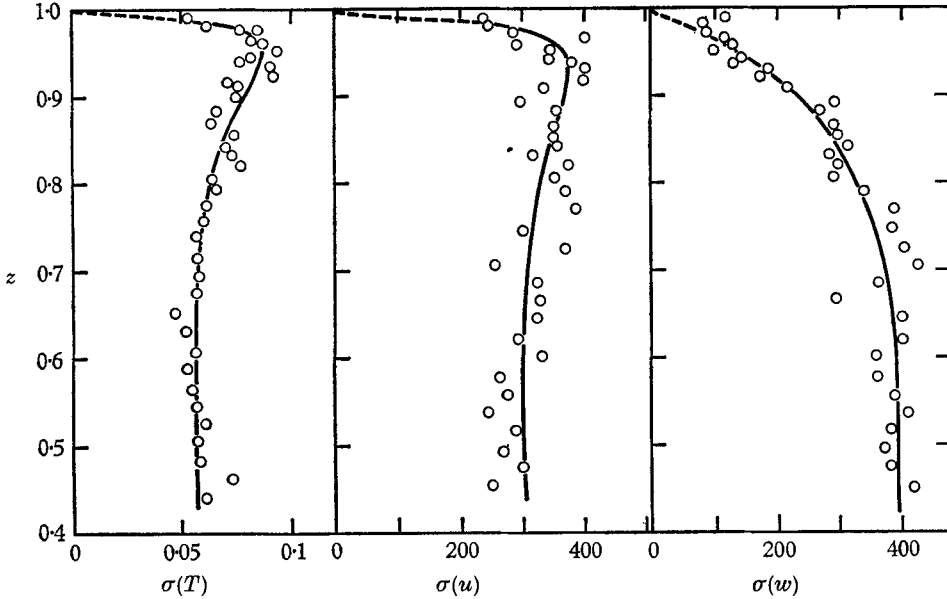


FIGURE 8. Vertical profiles of $\sigma(T)$, $\sigma(u)$ and $\sigma(w)$ at $Ra = 1.0 \times 10^7$.

The dotted curve in figure 6 is a profile of $\sigma(T)$ measured by Thomas & Townsend (1957) at the slightly larger Rayleigh number of $6.75 \times 10^5$. Their smaller values are presumably due to taking measurements at fixed points when a large, quasi-steady cell was present with lifetime much greater than the averaging periods. Thus, the contribution to $\sigma(T)$ from the largest scale eddy was largely absent. The dotted profile segment of figure 7 was measured by Somerscales (1965) above the bottom plate of a convection chamber at $Ra = 2.0 \times 10^6$. Again the observations were taken at fixed points, and the averaging period of five minutes appears to have been much too small.

If the values for $\sigma(u)$ and $\sigma(w)$ of figures 6–8 are integrated vertically from $z = 0.5$ to $z = 1$, the following ratios of $\overline{\sigma}(w)$ to $\overline{\sigma}(u)$ of table 2 are obtained: the

| $Ra$ | $\overline{\sigma}(w)/\overline{\sigma}(u)$ |
|---|---|
| $6.3 \times 10^5$ | 1.14 |
| $2.5 \times 10^6$ | 1.07 |
| $1.0 \times 10^7$ | 0.99 |

TABLE 2

overbars here denote the vertical average. These results are in the same sense as the observations of Malkus (1954a), using acetone, that horizontal velocities

become larger than vertical velocities for $Ra \geqslant \sim 10^6$. However there does not seem to be any dramatic decrease of the ratio with increasing Rayleigh number.

Vertical profiles of kinetic energy, $\langle KE \rangle \equiv \frac{1}{2}(2\langle u^2 \rangle + \langle w^2 \rangle)$, are presented in figure 9. The tendency for a secondary maximum near the boundary, associated with the maximum in $\langle u^2 \rangle$, seems to become less pronounced or even to disappear as the Rayleigh number increases. This effect is associated with a smaller relative maximum in the $\sigma(u)$ profile with increasing Rayleigh number.
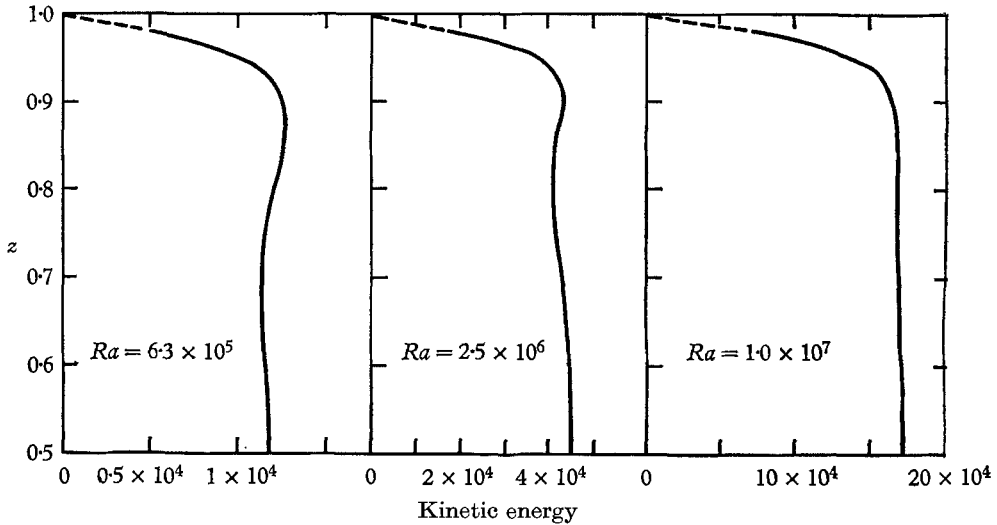
FIGURE 9. Vertical profiles of dimensionless kinetic energy at three Rayleigh numbers.
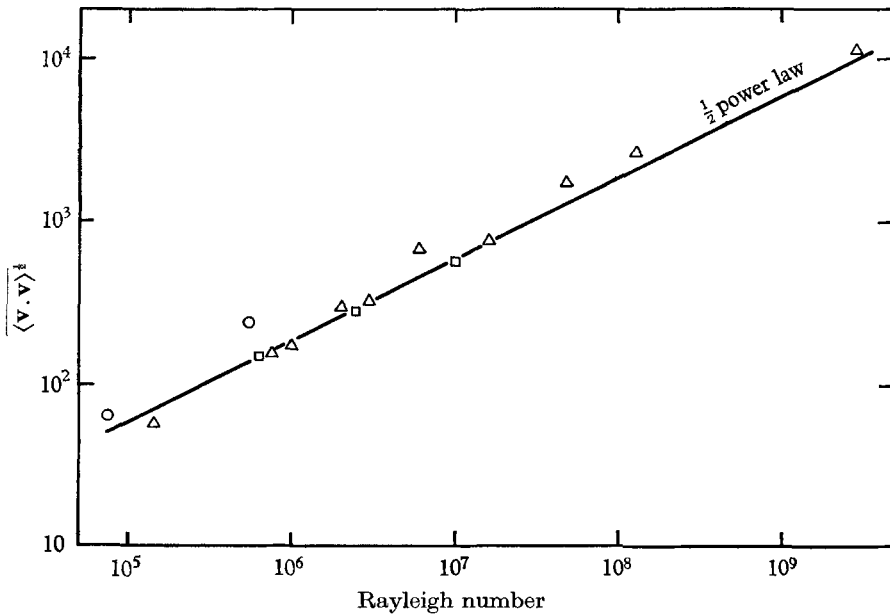
FIGURE 10. $\langle \mathbf{v} . \mathbf{v} \rangle^{\frac{1}{2}}$ as a function of Rayleigh number on a log-log plot. ◯, water (Malkus) $Pr = 7.0$; △, acetone (Malkus) $Pr = 3.7$; □, air (present results) $Pr = 0.71$.

Vertically averaged values of $\langle 2KE \rangle^{\frac{1}{2}} \equiv \langle \mathbf{v} . \mathbf{v} \rangle^{\frac{1}{2}}$ are shown by squares in figure 10 as a function of Rayleigh number. All other data points are values from the measurements of Malkus (1954*a*) obtained from his table 1. In plotting these additional data points, for which velocities have been made dimensionless by $\kappa_m/h$, the values taken for $\kappa_m$ (not reported by Malkus) are $1.04 \times 10^{-3}$ cm²/sec for acetone and $1.43 \times 10^{-3}$ cm²/sec for water. The values obtained here for air
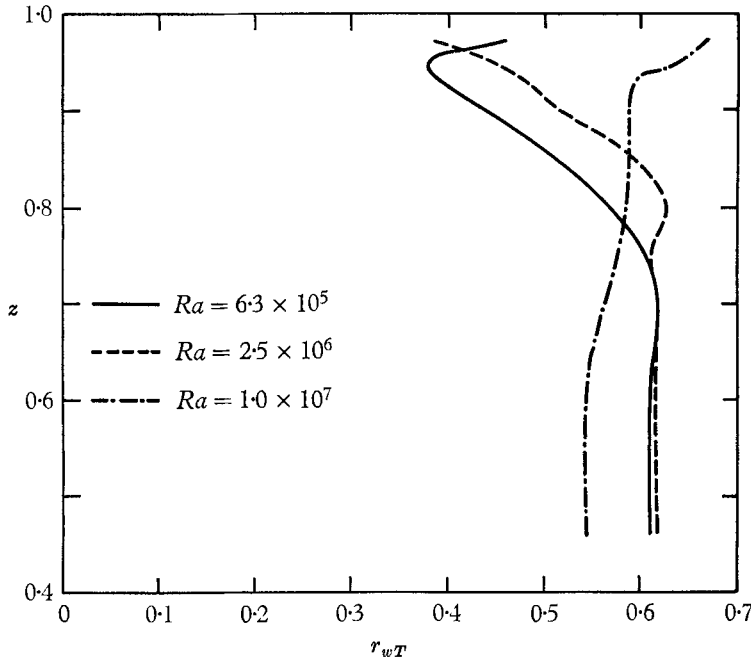


FIGURE 11. Vertical profiles of $r_{wT}$ for three Rayleigh numbers.

agree well with Malkus' measurements in acetone, but not so well with those in distilled water. However, in another paper Malkus (1954*b*) presents in his figure 2 a plot almost identical to our figure 10 in which his data points all fall near the same straight line. In spite of the discrepancy, which appears to involve an uncertainty in $\kappa_m$ for acetone, the additional data points for air help confirm Malkus' (1954*b*) theory, which predicts that $\langle \mathbf{v} . \mathbf{v} \rangle^{\frac{1}{2}}$ is proportional to $(Ra)^{\frac{1}{2}}$. (The solid line in figure 10 has the slope $\frac{1}{2}$.) The use of $\kappa_m/h$ to render velocities dimensionless thus appears to produce values which are not very sensitive to the Prandtl number, just as the Nusselt number is only a weak function of Prandtl number according to (13).

Concerning assumption (5), the slightly impure hot-wire signal $\tilde{u}$ was examined for its kurtosis $\langle \tilde{u}^4 \rangle / \langle \tilde{u}^2 \rangle^2$. An average value of about $2.7$, instead of 3, was obtained at all three Rayleigh numbers. No height dependence was detectable within the data scatter of $\pm 0.5$.

Values of $\bar{\sigma}(T)$ for air for the Rayleigh numbers of this study may be expressed as

$$\bar{\sigma}(T) = 0.38\, Ra^{-0.11}. \tag{12}$$

44-2

The product of $\overline{\langle \mathbf{v}.\mathbf{v}\rangle^{\frac{1}{2}}}$ and $\overline{\sigma}(T)$ consequently varies with Rayleigh number to a power of about 0·39 at these Rayleigh numbers, whereas from (11), $Nu \approx \langle wT \rangle$ varies with an exponent of about 0·33. The difference appears associated mainly with the slow relative increase of $\overline{\sigma}(u)$ with respect to $\overline{\sigma}(w)$ noted in table 2, and not with changes in the correlation coefficient between $w$ and $T$. The latter co-efficient, $r_{wT}$, defined by

$$r_{wT} \equiv \langle wT \rangle / [\sigma(w)\,\sigma(T)], \tag{13}$$

did not change systematically with the Rayleigh numbers studied. Vertical pro-files of $r_{wT}$ are shown in figure 11. Their vertically averaged values are all about $0.58 \pm 0.03$. Values of $r_{wT}$ close to the boundary ($z > 0.9$) are not to be trusted, however, because both numerator and denominator of (13) are then small.

## 5. Longitudinal spectra

Power spectra of $\tilde{u}$, $\tilde{w}$ and $T$ with respect to wavelengths in the longitudinal chamber direction are shown in figures 12, 13 and 14 on log-log plots for the three Rayleigh numbers. The analysis was by the method described in §3, with effects
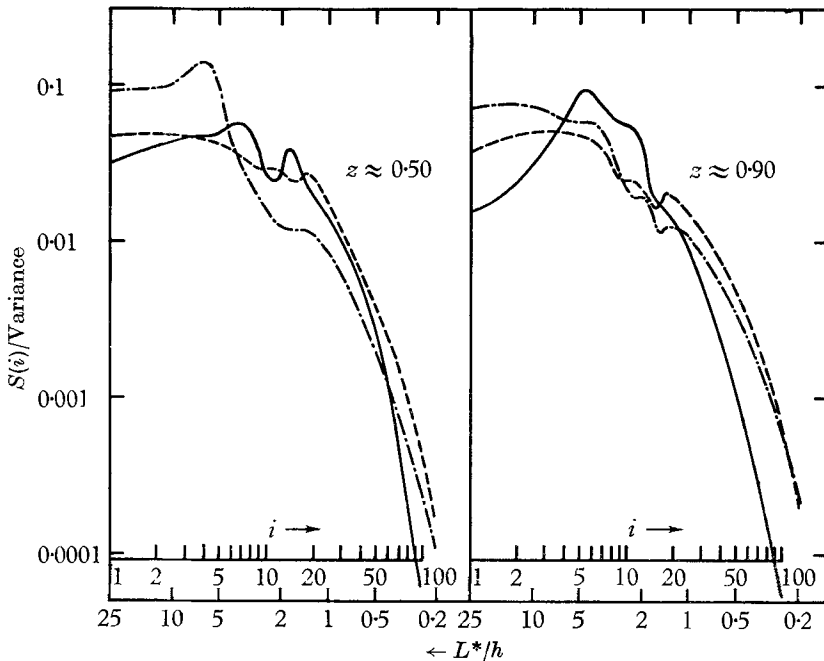


FIGURE 12. Normalized spectra of $\tilde{u}$, $\tilde{w}$ and $T$ at two heights for $Ra = 6.3 \times 10^5$ on log-log plots. ———, $\tilde{u}$; – – –, $\tilde{w}$; —·—, $T$.

of aliasing approximately removed. The effect of recorder damping is present in these spectra. The quantities $\tilde{u}$ and $\tilde{w}$ are proportional to the $X$-wire sum and difference signals, respectively, and are not exactly equal to the $u$ and $w$ velocity components as discussed in §3. In each figure spectral estimates $S(i)$ at a particular Rayleigh number are shown for the two heights centred near $z = 0.5$ and $0.9$,
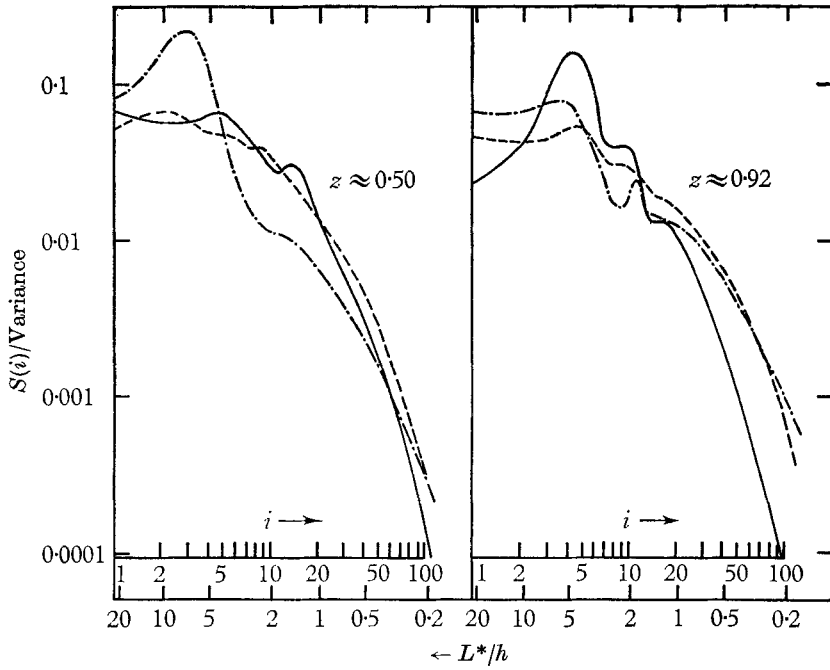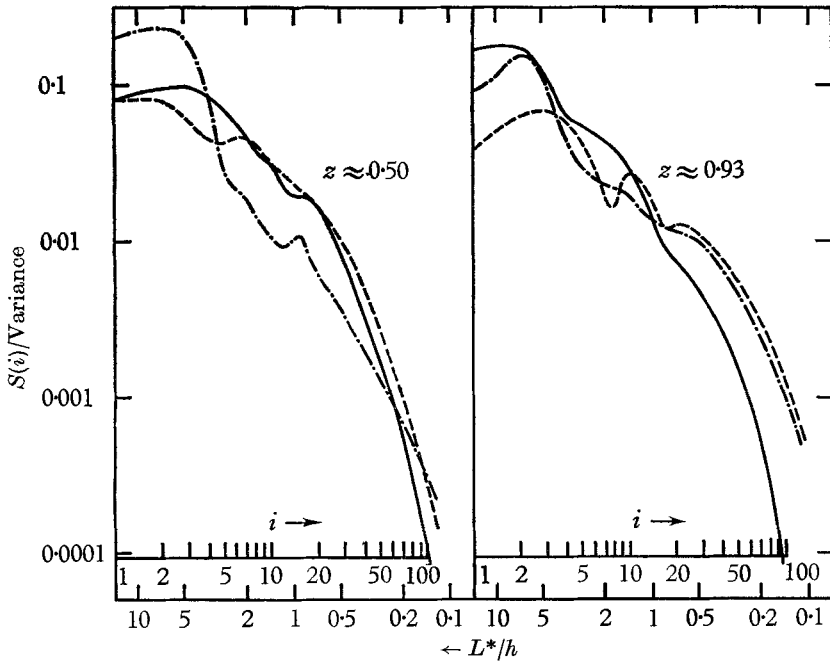
FIGURE 13. Normalized spectra of $\tilde{u}$, $\tilde{w}$ and $T$ at two heights for $Ra = 2\cdot5 \times 10^6$, on log-log plots. ——, $\tilde{u}$; ----, $\tilde{w}$; —·—, $T$.



FIGURE 14. Normalized spectra of $\tilde{u}$, $\tilde{w}$ and $T$ at two heights for $Ra = 1\cdot0 \times 10^7$, on log-log plots. ——, $\tilde{u}$; ----, $\tilde{w}$; —·—, $T$.

and are presented as a function of dimensionless, longitudinal wavelength $L^*/h \equiv L$. The Fourier harmonic number $i$ is included on the abscissa. The spectra are normalized with respect to the total variance, so that a summation over $i$ should yield unity, Individual, averaged spectral data points are not included because there was little scatter after averaging together the results of 8 traverses.

In general, these figures show a broad maximum in intensity to reside in the long waves $(L > 5)$ and a weak secondary maximum at moderate wavelengths $(0\cdot7 < L < 1\cdot7)$ at $z = 0\cdot5$. Two such secondary maxima are usually evident at $z = 0\cdot9$. They occurred so persistently in the individual spectra, as well as in the averaged ones presented, that we believe them to be statistically significant. On a plot in which equal areas contribute equally to the variance, these secondary maxima would be as pronounced as the primary ones. The wavelengths which divide the total variances into two equal parts occur for $1\cdot5 < L < 4$.

There is a trend for the position of the primary maxima to shift toward larger wavelengths as the Rayleigh number increases. Such a tendency may be hindered by the decreasing values of transverse aspect ratio (see table 1) as the Rayleigh number increases. That is, wavelengths in the $x$-direction may be limited in intensity by a tendency for large, energetic structures or cells to have equal lengths in both horizontal directions. In an earlier study (Deardorff & Willis 1965), the predominant large-scale wavelength in the direction of the greatest horizontal chamber dimension was shown to be a function of the aspect ratio of the smallest horizontal dimension, for aspect ratios less than about 10. Therefore, we believe that much larger transverse aspect ratios are necessary than those obtained here before the true wavelengths of the spectral components of maximum intensity can be reliably estimated.

There is a definite trend for the secondary maxima to shift toward shorter wavelengths as the Rayleigh number increases.

Concerning differences in the spectra at the different heights, a superposition of the two graphs at the larger two Rayleigh numbers would reveal greater intensity of longer waves and less of shorter waves at mid level than at $z = 0\cdot9$. This tendency is scarcely detectable at the smallest Rayleigh number.

The spectra of $T$, $\tilde{u}$ and $\tilde{w}$ are rather similar but show important differences. At $z = 0\cdot5$, the $\tilde{w}$ and $\tilde{u}$ spectra are most similar, while the temperature spectrum has more intensity in the longer waves and less in the moderate waves. The opposite result might be expected that the $\tilde{w}$ and $T$ spectra should be the more similar at mid level because of their positive correlation.

At $z = 0\cdot9$, the $\tilde{w}$ and $T$ spectra are the most similar, while the $\tilde{u}$ spectrum has more intensity in the moderate wavelengths and less in the shorter wavelengths. The difference between $\tilde{u}$ and $\tilde{w}$ spectra here is to be expected if regions of significant horizontal velocities are stretched out, or horizontally 'mushroomed', near the boundary with consequent horizontal squeezing and vertical distension of the significant vertical motions.

At much larger Rayleigh numbers, an inertial subrange could be expected to commence beyond the secondary maxima and extend to shorter wavelengths. At the Rayleigh numbers studied here, most of the dissipation by molecular viscosity appears to occur for scales of $0\cdot1 < L < 1$. These scales are not sufficiently

removed from the main energy bearing scales of $0.5 < L < 10$ to allow an inertial subrange.

Cospectra of $\tilde{w}T$, normalized by $\langle \tilde{w}T \rangle$, are shown by the upper set of curves in figure 15 for $z = 0.5$, where $C_{wT}$ is the cospectral intensity. Although small negative values were occasionally obtained in some individual spectral products, the average values from 8 traverses were positive for all $L$. The secondary maxima
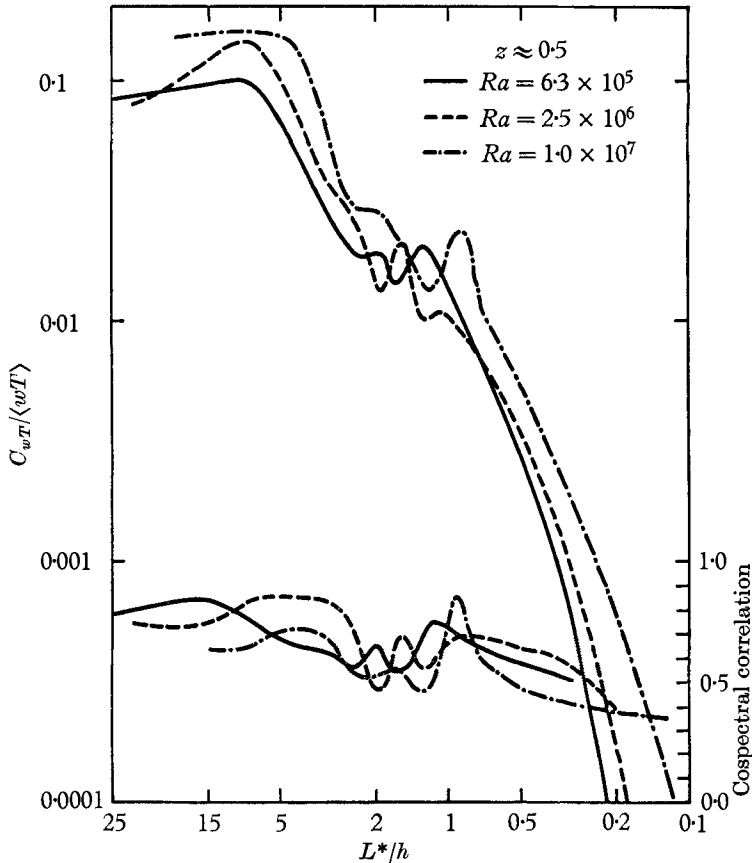


FIGURE 15. Normalized cospectra of $\tilde{w}$ and $T$ for $z = 0.5$ at three Rayleigh numbers, upper curves. Lower curves are co-spectral correlation coefficients with ordinate on the right.

here consist of double peaks, whereas this occurred for the individual spectra most noticeably at $z = 0.9$. Correlation coefficients between $\tilde{w}$ and $T$ on a spectral basis are shown by the lower set of curves. They are defined by

$$r_{wT}(i) \equiv C_{wT}(i)/[S_T(i)S_w(i)]^{\frac{1}{2}}.$$

The secondary peaks in the cospectra are seen to be associated with strong peaks in the cospectral correlation. The correlation generally decreases with increasing $L$, but surprisingly slowly. A re-plot of figure 15 upon an equal-area, equal-covariance graph would reveal that 90 % of the heat flux is carried by waves of length $L$ greater than 0.7, 0.5 and 0.4 for the respective Rayleigh numbers in increasing order.

## 6. Balance of thermal and kinetic variance equations

Some of the most enlightening measurements of turbulence are of individual terms in the averaged thermal variance and turbulent kinetic energy equations. The relative contributions of different processes toward a balance in the production and destruction of the variance may then be examined.

### 6.1. *Thermal variance equation*

If the diffusion equation for the dimensionless temperature fluctuation is multiplied by the fluctuation and averaged longitudinally, the result for this horizontally homogeneous case is

$$\frac{\partial}{\partial t}\left\langle \frac{T'^2}{2} \right\rangle = -\langle wT \rangle \left\langle \frac{\partial T}{\partial z} \right\rangle - \frac{\partial}{\partial z}\left\langle \frac{wT'^2}{2} \right\rangle - \left\langle \frac{\partial T'}{\partial x_i}\frac{\partial T'}{\partial x_i} \right\rangle + \frac{\partial^2}{\partial z^2}\left\langle \frac{T'^2}{2} \right\rangle \quad (i = 1, 2, 3).$$

(14)

The left-hand side of (14) is zero for the steady state, but its formal inclusion determines whether individual terms on the right are contributing towards a production or a destruction of $\langle T'^2 \rangle$.

The first term on the right may be called the 'production' term because both $\langle wT \rangle$ and $\langle -(\partial T/\partial z) \rangle$ have been seen to be generally positive. It was evaluated from measurements of both these terms, with the restriction that its maximum value was adjusted to $(Nu)^2/4$. This maximum value can be shown to be a consequence of the constancy with height of the total heat flux. For this purpose the Nusselt number was taken as the vertical average of the measured values shown in figure 5.

The second term on the right may be called the 'diffusion' term and represents a diffusion of thermal variance by the turbulent elements. It was evaluated by graphical differentiation of the smoothed curves of $\langle wT'^2 \rangle/2$ presented in figure 16. The curves have been drawn through the origin at $z = 0.5$ from symmetry considerations. The scatter due to sampling error is quite large, and poor accuracy is to be expected in the vertical derivative close to the boundary where a reversal in sign apparently occurs. This reversal is considered real as it was predicted by numerical models of Deardorff (1964, 1965).

Negative values of $\langle wT'^2 \rangle$ near $z = 0.7$ to $0.9$ are related to the negative skewness of the temperature fluctuations previously discussed. Because of the positive correlation between $w$ and $T$, this negative skewness also leads to negative $\langle wT'^2 \rangle$ in this region. In the vicinity of $z = 0.1$ to $0.3$ the signs of the skewness and of $\langle wT'^2 \rangle$ would be reversed so that the diffusion term $-(\partial/\partial z)\langle wT'^2/2 \rangle$ is positive throughout the central region. Hence the magnitude and sign of the diffusion term in the central region appears to be largely controlled by the motions much nearer the boundaries which are responsible for the existence of narrow plumes extending from the boundaries. The relative narrowness of plumes emanating from the vicinity of a given plate may in turn be caused by the pinching effect of mushroomed portions of contrasting, adjacent plumes which emanated from the vicinity of the opposite plate.

The third term on the right of (14) may be called a 'dissipation', as it always represents a rate of destruction or smoothing of thermal variance. The portion $\langle(\partial T'/\partial z)^2\rangle$ of this term was measured directly by the temperature-difference probe described in §2.3, while the remaining portion $2\langle(\partial T/\partial x)^2\rangle$ was measured by $x$-differentiation of longitudinal temperature traces. However, a positive
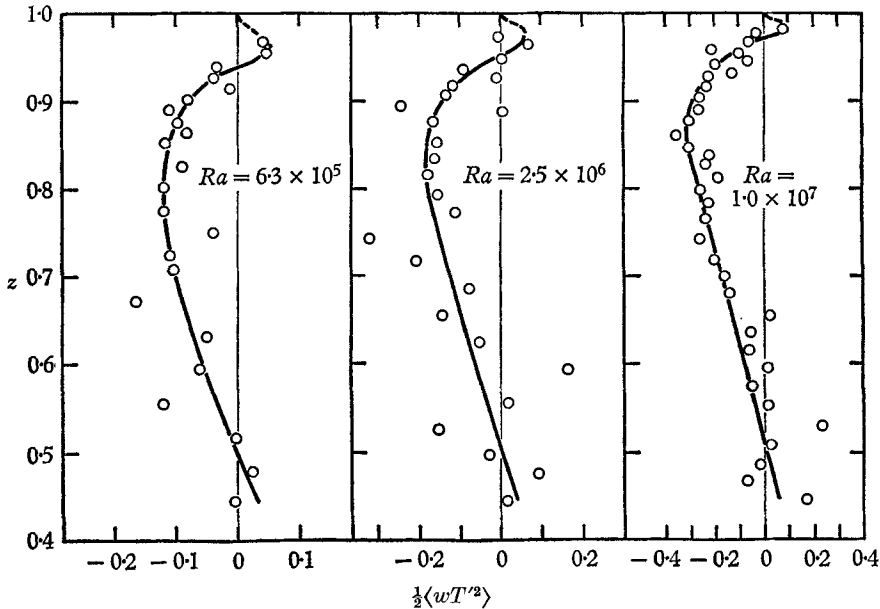


FIGURE 16. Vertical profiles of $\frac{1}{2}\langle wT'^2\rangle$ at three Rayleigh numbers.

correction in the range from 20 to 100 % had to be applied to this term to account for combined effects of finite-difference and recorder damping. The corrections were estimated from extrapolations of the spectra of figures 12, 13 and 14.

The last term in (14) may be called a molecular-transfer term which tends to transfer or redistribute extreme values of $\langle T'^2\rangle$, but at the slow molecular rate which is generally negligible with respect to other processes except very close to a boundary. It was obtained from double differentiation of $\sigma(T)$ curves of figures 6, 7 and 8.

The four terms on the right of (14) are shown as functions of height in figures 17, 18 and 19 for the three Rayleigh numbers. All three figures show that near the boundary the diffusion, dissipation and transfer terms are all important in balancing the large production term. In the central region the diffusion and thermal dissipation terms are the main ones which tend to balance. Hence the absence of an appreciable central temperature gradient (or potential temperature gradient) is to be 'explained' by the importance of the diffusion term in this region.

The increase of the thermal dissipation as the boundary is approached is first due to increased values of $\langle(\partial T/\partial x)^2\rangle$ and then of $\langle(\partial T'/\partial z)^2\rangle$. The former term reaches a maximum where $\sigma(T)$ is a maximum, and the combined dissipation seems to approach a nearly constant value at the boundary. Extremely close to

the boundary the thermal dissipation must be balanced only by the molecular transfer term. In figure 17 these boundary values could be estimated because the linear variation of $\sigma(T)$ near the boundary in figure 6 could be estimated. At the higher Rayleigh numbers the boundary slopes of the $\sigma(T)$ curves could not be closely estimated, and asymptotic boundary values of the transfer and dissipation terms are not presented.
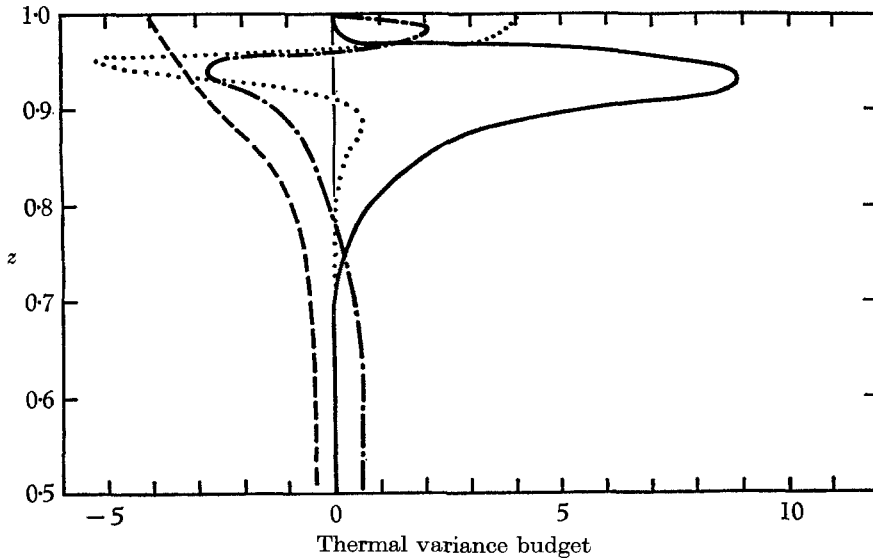


FIGURE 17. Vertical profiles of terms in thermal variance equation at $Ra = 6\cdot3 \times 10^5$.
——, production, $-\langle w'T'\rangle\langle\partial T/\partial z\rangle$; ----, thermal dissipation, $-\langle(\partial T/\partial x)^2 + (\partial T/\partial y)^2 + (\partial T'/\partial z)^2\rangle$; ······, molecular transfer, $\partial^2\langle\frac{1}{2}T'^2\rangle/\partial z^2$.



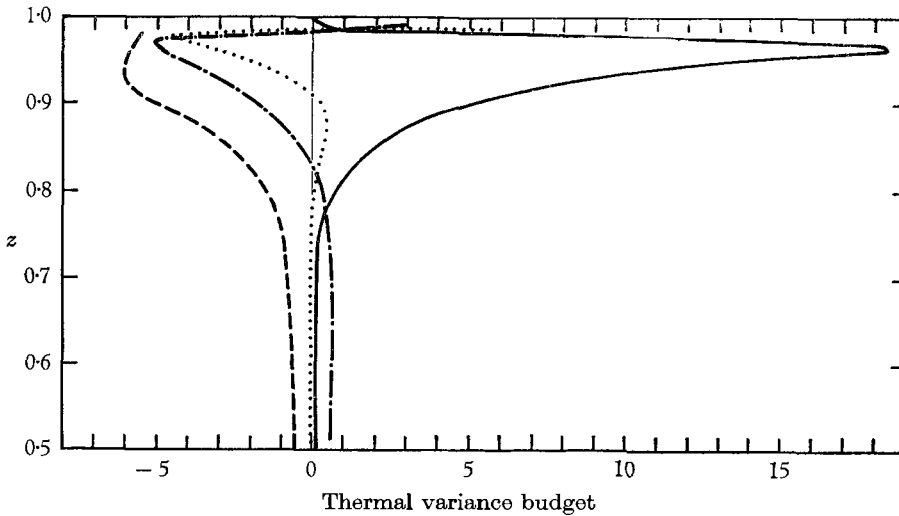FIGURE 18. Vertical profiles of terms in thermal variance equation at $Ra = 2\cdot5 \times 10^6$.
——, production; ----, thermal dissipation; ······, molecular transfer; —·—, diffusion.

Although individual terms in figures 17, 18 and 19 behave in a reasonable fashion and tend to sum to zero, inspection of the residuals discloses that individual terms may have errors on the order of $\pm 50\%$ in the boundary regions. In figure 20 the residuals have been divided by the height-dependent thermal dissipation. Normalized residuals as large as unity in the boundary-layer region probably result largely from sampling error combined with the effect of vertical
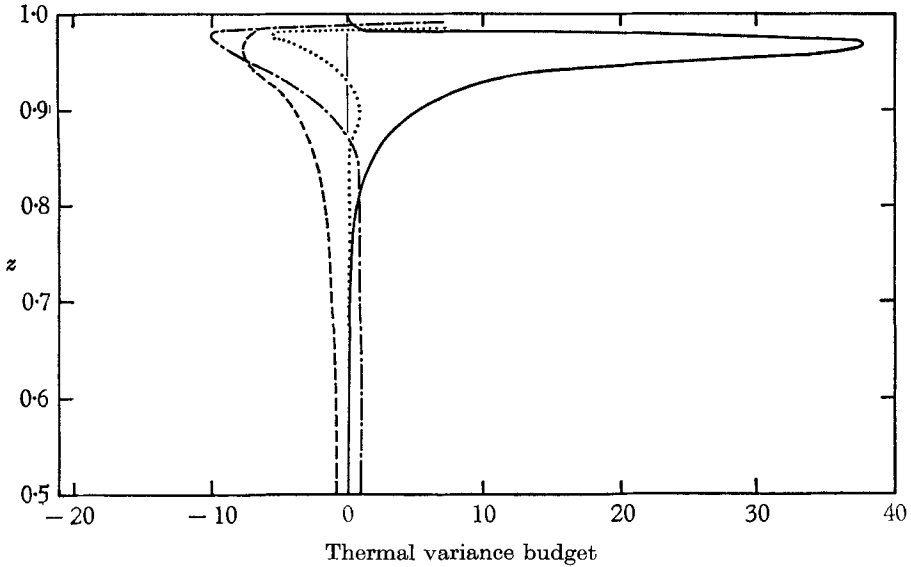


FIGURE 19. Vertical profiles of terms in thermal variance equation at $Ra = 1 \cdot 0 \times 10^{7}$. ———, production; ———, thermal dissipation; ······, molecular transfer; —·—, diffusion.
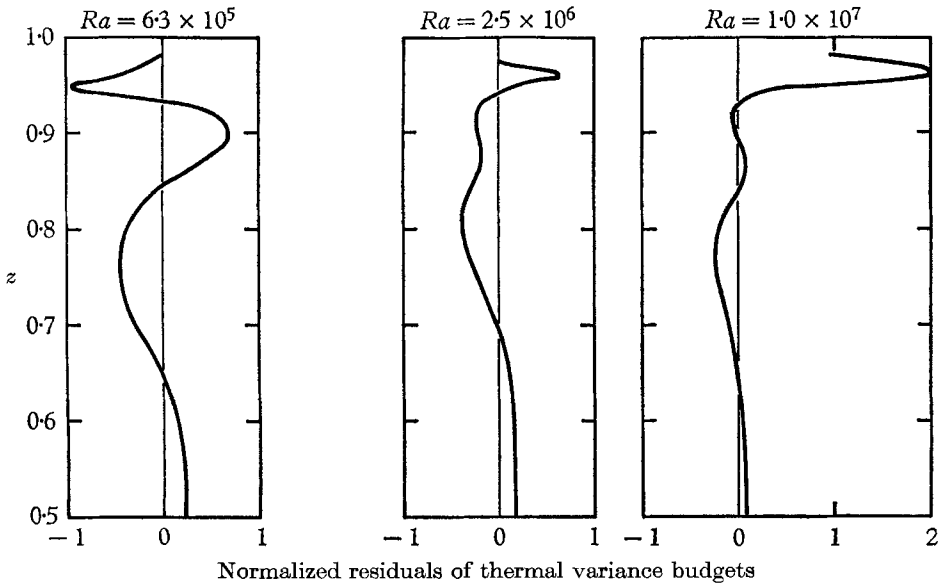


FIGURE 20. Residuals of figures 17, 18 and 19, normalized by the height-dependent thermal dissipation.

differentiation of the estimated curves. The very large imbalance at $z = 0.96$ at the largest Rayleigh number seems attributable mainly to gross underestimation of the diffusion term here. Because of the vertical separation of the temperature and velocity sensors, a relatively large positive value of $\langle wT'^2 \rangle$ may well have existed at $z = 0.98$ (see figure 16) and not have been resolved instrumentally. A larger reversal at this level would then have led to a more negative diffusion term at $z = 0.96$. In addition, the exact level of the large and sharp maximum of the production term is somewhat uncertain.

### 6.2. *Kinetic energy balance*

If the Navier–Stokes equations (with the Boussinesq approximation) for the dimensionless velocity components are multiplied by the respective components, added together, and averaged longitudinally, the result for the horizontally homogeneous case is

$$\frac{\partial}{\partial t} \langle (KE) \rangle = Pr.Ra\langle wT \rangle - \frac{\partial}{\partial z} \langle w(KE+p) \rangle$$

$$- Pr \left\langle \frac{\partial u_i}{\partial x_j} \frac{\partial u_i}{\partial x_j} \right\rangle + Pr \frac{\partial^2}{\partial z^2} \langle KE \rangle \quad (i = 1, 2, 3; j = 1, 2, 3), \quad (15)$$

where $p$ is the dimensionless pressure fluctuation. The first term on the right is the production term. The second is the diffusion term in which pressure fluctuations may contribute. The third is essentially the rate of dissipation of kinetic energy, and the last is the molecular transfer term.

The production term here is much more accurately known than is the corresponding term in the thermal variance equation. However, the diffusion term in (15) is much more difficult to measure because of well known difficulties in measuring static pressure fluctuations of small amplitude. Difficulties were also encountered in attempts to measure $\langle w^3 \rangle$ reliably. Therefore the entire diffusion term was obtained as the residual of the other terms in the kinetic energy budget.

The dissipation term was estimated from finite-difference measurements of $\langle (\partial u/\partial x)^2 \rangle$ and $\langle (\partial w/\partial x)^2 \rangle$ along with use of assumptions (9f–m). Again, additive corrections ranging from 20 to 100 % were obtained from extrapolations of the spectra, and were applied to the squared derivatives.

The molecular transfer term was obtained by twice differentiating the kinetic energy curves of figure 9.

The results are presented in figures 21, 22 and 23 for the three Rayleigh numbers. The production is large and important outside of the boundary layer and is balanced mainly by the dissipation. The diffusion term obtained as a residual must obviously have a positive peak near the boundary to help counterbalance the dissipation and molecular transfer terms there. The fact that it is negative throughout the central region is then a gross check of the reliability of the other terms, for the vertical integral of the diffusion term over the full distance between plates or over either half must be zero from boundary-value and symmetry considerations. This condition was not quite obtained, however, from the original data and corrected dissipation. In order to force this condition, the dissipation

term was re-corrected in magnitude at all levels by percentage increases of 11 and 1, respectively, at $Ra = 2\cdot5 \times 10^6$ and $1\cdot0 \times 10^7$.

The changed shape of the dissipation profile near the boundary at the largest Rayleigh number may be a spurious result of too many assumptions and corrections. However, it resulted from smaller relative contributions of the assumed
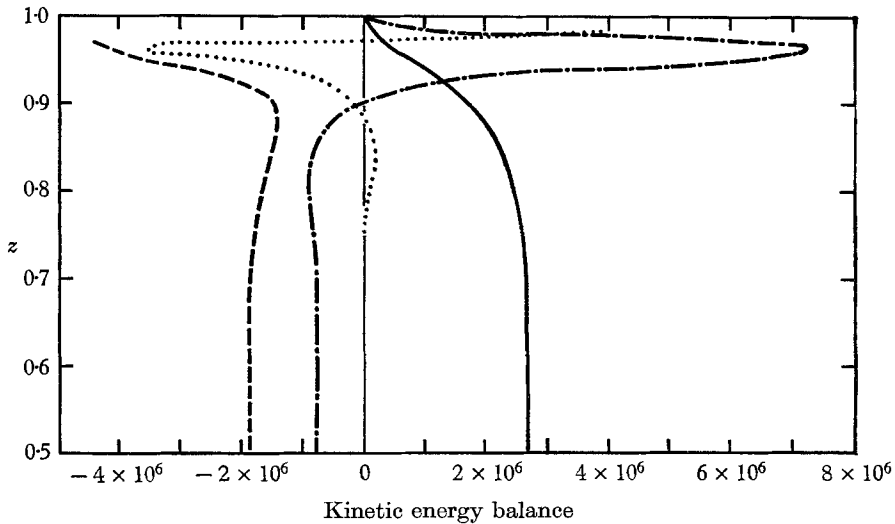


FIGURE 21. Vertical profiles of terms in kinetic energy equation at $Ra = 6\cdot3 \times 10^5$. ——, production, $Pr.Ra\langle wT\rangle$; ———, dissipation, $-Pr\langle \partial u_i/\partial x_j \partial u_i/\partial x_j\rangle$; ······, molecular transfer, $\partial\langle KE\rangle/\partial z$; —·—, diffusion (residual), $-\partial/\partial z\langle w(p+u^2+(w/2)^2)\rangle$.
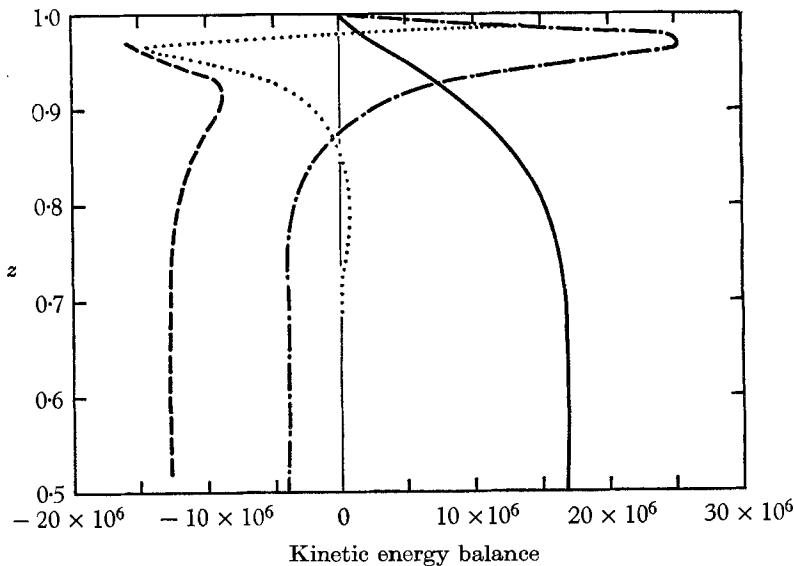


FIGURE 22. Vertical profiles of terms in kinetic energy equation at $Ra = 2\cdot5 \times 10^6$. ——, production; ———, dissipation; ······, molecular transfer; —·—, diffusion.

vertical gradients near the boundaries, along with the absence of a significant maximum of $\langle(\partial u/\partial x)^2\rangle$ in the boundary layer at the largest Rayleigh number. The latter feature could be due to increased horizontal spreading of the horizontal velocity eddies near the boundary. At much larger Rayleigh numbers, when the dissipation would not be closely associated with the energy bearing motions, a pronounced increase of dissipation in the boundary layer would be expected.
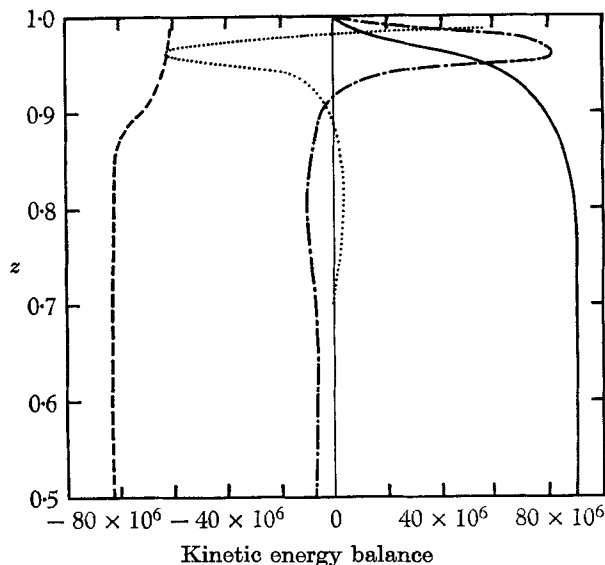


FIGURE 23. Vertical profiles of terms in kinetic energy equation at $Ra = 1 \cdot 0 \times 10^7$.
——, production; — — —, dissipation; · · · · · ·, molecular transfer; —·—, diffusion.

Another unusual result obtained is that $\langle(\partial w/\partial x)^2\rangle$ is about five times larger than $\langle(\partial u/\partial x)^2\rangle$ in the central region, instead of being twice as large if motions were fully isotropic. Also, $\langle(\partial T/\partial x)^2\rangle$ was found to be about 1·7 times larger than $\langle(\partial T'/\partial z)^2\rangle$ in the central region. Again we attribute these disparities from iso-tropy to vertical elongation of vertical velocity and temperature structures, which would correspond to plume-like structures.

| $Ra$ | $\lambda_{KE}^*/h$ | $\lambda_T^*/h$ | $\eta^*/h$ |
|---|---|---|---|
| $6 \cdot 3 \times 10^5$ | 0·21 | 0·37 | 0·021 |
| $2 \cdot 5 \times 10^6$ | 0·16 | 0·27 | 0·013 |
| $1 \cdot 0 \times 10^7$ | 0·12 | 0·19 | 0·008 |

TABLE 3

Some microscales associated with dimensionless rates of dissipation of kinetic energy and thermal variance in the central region are given in table 3 even though the motions are not three-dimensionally isotropic. These have been defined as

$$\lambda_{KE}^*/h \equiv (10 \cdot Pr \cdot \langle KE\rangle/\epsilon_K)^{\frac{1}{2}},$$
$$\lambda_T^*/h \equiv (9\langle T'^2\rangle/\epsilon_T)^{\frac{1}{2}},$$
$$\eta^*/h \equiv (Pr^3/\epsilon_K)^{\frac{1}{4}},$$

where $\lambda_{KE}^*$ and $\lambda_T^{*|}$ are Taylor microscales associated with dimensionless rates of dissipation of kinetic energy, $\epsilon_K$, and of thermal variance, $\epsilon_T$, respectively; and $\eta^*$ is the Kolmogoroff length scale.

Although the Kolmogoroff scale presumably has little significance at these rather small Rayleigh numbers, its smaller magnitude than the Taylor microscales here is also typical of turbulence with an inertial subrange (Hinze 1959, p. 184).

## 7. Concluding remarks

Qualitative explanations have been put forth during presentation of the results for many of the interesting features observed. The Rayleigh numbers studied are far too large for detailed explanations based upon linear theories to be of much use, and are probably far too small for similarity theories to be applicable. Good quantitative explanations probably await fully non-linear and three-dimensional numerical integrations of the basic equations. It is hoped that the results presented here will be of value to theoretical studies of this nature in spite of the experimental limitations imposed mainly by presence of side walls of the convection chamber. Improved measurements over those presented here could best be obtained in future experiments by use of an even larger convection chamber, and by more accurate estimates of the rate of dissipation of kinetic energy.

REFERENCES

COLLIS, D. C. & WILLIAMS, M. J. 1959 Two-dimensional convection from heated wires at low Reynolds numbers. *J. Fluid Mech.* **6**, 357–384.

DEARDORFF, J. W. 1964 A numerical study of two-dimensional parallel-plate convection. *J. Atmos. Sci.* **21**, 419–438.

DEARDORFF, J. W. 1965 A numerical study of pseudo three-dimensional parallel-plate convection. *J. Atmos. Sci.* **22**, 419–435.

DEARDORFF, J. W. & WILLIS, G. E. 1965 The effect of two-dimensionality on the suppression of thermal turbulence. *J. Fluid Mech.* **23**, 337–353.

DEARDORFF, J. W. & WILLIS, G. E. 1967 The free-convection temperature profile. *Quart. J. Roy. Meteor. Soc.* **93** (to be published).

GLOBE, S. & DROPKIN, D. 1959 Natural convection heat transfer in liquids confined by two horizontal plates and heated from below. 1958 *Heat Trans. & Fluid Mech. Inst.* pp. 156–165. Berkeley, University of California.

HINZE, J. O. 1959 *Turbulence.* New York: McGraw-Hill.

KING, L. V. 1914 On the convection of heat from small cylinders in a stream of fluid. Determination of convection constants of small platinum wires with application to hot-wire anemometry. *Phil. Trans.* A **214**, 373–432.

MALKUS, W. V. R. 1954a Discrete transitions in turbulent convection. *Proc. Roy. Soc.* A **225**, 185–195.

MALKUS, W. V. R. 1954b The heat transport and spectrum of thermal turbulence. *Proc. Roy. Soc.* A **225**, 196–212.

SILVESTON, P. L. 1958 Wärmedurchgang in Waagerechte Flüssigkeitsschlichten. *Forsch. Ing. Wes.* **24**, 59–69.

SOMERSCALES, E. F. C. 1965 Experimental investigation of the temperature distribution in a horizontal fluid layer heated from below. Ph.D. Dissertation, Cornell University, Dept. Mech. Eng., available from University Microfilms Inc., Ann Arbor, Michigan.

THOMAS, D. B. & TOWNSEND, A. A. 1957 Turbulent convection over a heated horizontal surface. *J. Fluid Mech.* **2**, 473–492.
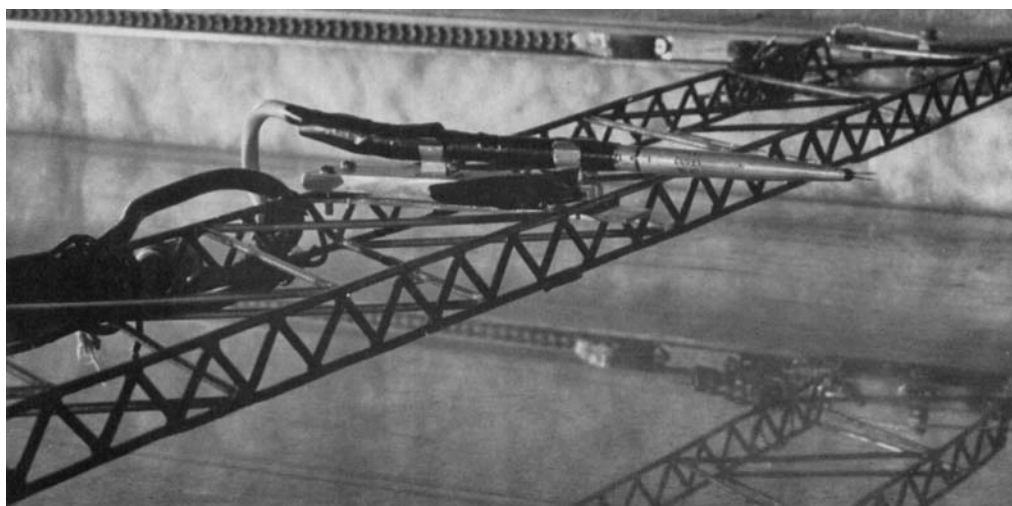
FIGURE 2. Photograph of the temperature-gradient probe mounted upon the support frame. Movement is from left to right during measurements.